Influence of use conditions on heat transfer in an insulated box equipped with a phase change material

Tanathep Leungtongkum, Denis Flick, Nattawut Chaomuang, Alain Denis, Onrawee Laguerre

Journal Pre-proof

Influence of use conditions on heat transfer in an insulated box equipped with a phase change material

Tanathep Leungtongkum, Denis Flick, Nattawut Chaomuang, Alain Denis, Onrawee Laguerre

PII: S0260-8774(23)00242-X

DOI: https://doi.org/10.1016/j.jfoodeng.2023.111644

Reference: JFOE 111644

To appear in: *Journal of Food Engineering*

Received Date: 26 April 2023

Revised Date: 18 June 2023

Accepted Date: 30 June 2023

Please cite this article as: Leungtongkum, T., Flick, D., Chaomuang, N., Denis, A., Laguerre, O., Influence of use conditions on heat transfer in an insulated box equipped with a phase change material, *Journal of Food Engineering* (2023), doi: https://doi.org/10.1016/j.jfoodeng.2023.111644.

CRediT author statement

Tanathep Leungtongkum: Conceptualization, Methodology, Investigation, Validation, Formal analysis, Software, Writing - Original Draft Preparation and Visualization

Denis Flick: Methodology, Validation, Formal analysis, Writing - Review & Editing and Supervision.

Nattawut Chaomuang: Conceptualization, Methodology, Investigation, Validation, Formal analysis, Software, Writing - Original Draft Preparation, Visualization and Funding acquisition

Alain Denis: Investigation and Software

Onrawee Laguerre: Validation, Formal analysis, Writing - Review & Editing, Supervision, Project Administration, Funding acquisition

Influence of Use Conditions on Heat Transfer in an Insulated Box Equipped with a Phase Change Material

Tanathep Leungtongkum[a, b]*, Denis Flick[b], Nattawut Chaomuang[c], Alain Denis[a] and Onrawee Laguerre[a]

[a]Université Paris-Saclay, INRAE, FRISE, 92761 Antony, France

[b]Université Paris-Saclay, INRAE, AgroParisTech, UMR SayFood, 91120 Palaiseau, France

[c]Department of Food Engineering, School of Engineering, King Mongkut's Institute of Technology Ladkrabang, Bangkok, Thailand 10520

***Corresponding author:** Tanathep Leungtongkum, e-mail: Tanathep.leungtongkum@inrae.fr

Highlights

- Temperature and air velocity fields (by PIV) in insulated boxes with PCM were shown
- The effect of box configurations and operating conditions was studied
- PCM at the top allows 1.1°C lower maximum product temperature than that on the side
- An air gap of 20 mm below the product does not change the temperature profile
- Results can be used for optimizing the box and the condition for food transport

Abstract

An insulated box with Phase Change Material (PCM – ice, melting point ~ 0°C) and loaded by test product (Tylose) was investigated experimentally to study the effect of the PCM position, Aspect Ratio (AR = height/width) of box, ambient temperature, initial test product temperature and spacing beneath the test product. The temperature and the air velocity measured by thermocouples and Particle Image Velocimetry (PIV), respectively, were analyzed under stable conditions. The maximum product temperature was lower for PCM at the top (6.6°C, AR ≈ 1) than for PCM on a sidewall (7.7°C, AR ≈ 1) and increased with AR (9.9°C, AR ≈ 1.7). A non-linear relation between ambient temperature and product temperature was observed with the maximum product temperature from 5.2°C (10°C ambient) to 9.1°C (30°C ambient). The influence of spacing beneath the product was negligible despite different airflow patterns. Simple equations were proposed to predict the maximum storage time and mean temperature in the box enabling us to study the influence of PCM and product mass, melting point, box insulation and ambient temperature.

Keywords: Insulated box, Phase Change Material, Airflow, Heat Transfer, Food Cold Chain

Nomenclature

A	Exchange area [m^2]
AR	Aspect ratio of box = height/width [-]
C_p	Specific heat [J·kg^{-1}·K^{-1}]
e	Wall thickness [m]
h	Convective heat transfer coefficient [W·m^{-2}·K^{-1}]
L	Characteristic length [m]
L_f	Latent heat of fusion of PCM [J·kg^{-1}]
$\dot{m}$	Mass flow rate of air [kg·s^{-1}]
m	Mass [kg]
t	Time [s]
t_{max}	Maximum storage time [s]
T	Temperature [°C]
T_m	Melting temperature of PCM (~ 0°C)
T_{amb}	Ambient temperature [°C]

T^* Dimensionless temperature = $\frac{T - T_m}{T_{amb} - T_m}$ [-]

ΔT Largest temperature difference [°C]

U Overall heat transfer coefficient between ambient and product surface through box insulation [W·m^{-2}·K^{-1}]

x, y, z Coordinate [m]

Greek letters

α_c Dimensionless heat transfer coefficient at cold wall = $exp\left(-\frac{A_c h_c}{\dot{m} C_{p,air}}\right)$ [-]

α_w Dimensionless heat transfer coefficient at warm walls = $exp\left(-\frac{A_w U}{\dot{m} C_{p,air}}\right)$ [-]

β Ratio of thermal resistance at cold and at warm walls = $\frac{A_w U}{A_c h_c}$ [-]

ρ Density [kg·m^{-3}]

τ Thermal time constant [s]

λ Thermal conductivity [W·m^{-1}·K^{-1}]

Subscript

air Air

ave Average value

c Cold surface/walls

ini Initial value

max Maximum value

min Minimum value

p Product

pcm Phase change material

w Warm surface/walls

1. Introduction

Insulated boxes equipped with a Phase Change Material (PCM) are attracting particularly for the last mile delivery of small quantities of temperature-sensitive food and pharmaceutical products. This is due to the simple implementation, low cost and flexibility related to several box designs with different volumes ranging from 5 L to more than 300 L. Several parameters have an influence on the internal temperature profiles such as box characteristics (dimensions, aspect ratio, insulation), PCM (melting point, mass, position), product (thermal properties, mass, compactness) and operating condition (ambient temperature, transport duration). Because of the complex interactions between these parameters, they need to be considered together to avoid temperature abuse during delivery.

The temperature evolution inside an insulated box equipped with PCM loaded by real food/food model was investigated experimentally and numerically by several authors and summarized in Leungtongkum et al. (2022). In general, the product located at the corners of the box has the highest temperature (Laguerre et al., 2018; Margeirsson et al., 2012). Du et al. (2020) have compared the effect of PCM at the top, bottom, and all sidewalls on internal temperature evolution. The authors found that placing PCM at the bottom generated the highest internal temperature and the highest temperature difference between the min and max values. For high-value products like vaccines, five or six PCM plates are placed on the box walls to directly compensate the heat losses through the walls by PCM melting. This allows assuring the preservation of the recommended temperature (Kacimi & Labranque, 2019) but the useful volume for the product is significantly reduced, thus, this practice may not be suitable for low cost product like food.

For simplification purposes, several studies assumed conduction only in the air, the product and the wall (Du et al., 2020; Paquette et al., 2017; Xiaofeng & Xuelai, 2021). To represent the real phenomena, Rincón-Casado et al. (2017) developed a numerical model considering conduction and natural convection to predict the temperature profile and airflow pattern in an empty cavity while Leporini et al. (2018) also took radiation into account. Recently, some numerical studies considered natural convection of internal air and of melted PCM (Burgess et al., 2022; Calati et al., 2022; Rahimi-Khoigani et al., 2023).

Various phenomena are involved simultaneously in an insulated box equipped with PCM: conduction inside the product, the PCM and the walls of the box, convection between air and product/PCM, and between the external air and the box, radiation between walls, phase change during PCM melting and food quality evolution. Under natural convection as that in an insulated box, these three heat transfer modes (conduction, convection and radiation) are of the same order of magnitude in terms of heat flux (Laguerre & Flick, 2004). However, only a few studies considered all of them according to the difficulty in measuring low air velocities (Miroshnichenko & Sheremet, 2018). In fundamental studies of natural convection in a closed cavity, two walls are generally at imposed temperatures (cold and warm) while the other walls are adiabatic, and most of them investigated empty cavities (Leporini et al., 2018; Zhang et al., 2015). PCM was used as a thermal energy storage in an empty cavity (Labihi et al., 2017; Moreno et al., 2020). Choi et al. (2015) and Lee et al. (2016) conducted numerical studies of a rectangular cavity filled with a circular cylinder (cylinder diameter /cavity size = 0.125). Some studies have investigated cavities filled with a porous medium (particle diameter/box width < 0.01), e.g., Ataei-Dadavi et al. (2019). The results of these studies cannot be applied to our case where only one wall (PCM container) is at almost constant temperature and all the other walls of the box are non-adiabatic. Moreover, a porous medium approach is not appropriate to our study, since the ratio between product diameter and box width is ≥ 0.1, thus, different airflow pattern.

The strength of our work is that it is the first experimental study concerning the measurement of airflow patterns and air velocity in an insulated box with PCM at different locations by using an optical technique (PIV). Some results were already presented in a previous article (Leungtongkum et al., 2023a) for a limited number of configurations. The present article investigates many more parameters: aspect ratio, ambient temperature, initial product temperature and air gap underneath the product. From a practical point of view, this article also proposes simple equations to predict the maximum storage time, the equilibrium temperature and temperature heterogeneity at thermal stable condition enabling to study the influence of PCM mass, melting point, box insulation and ambient temperature. These equations are easy to use and they would be useful for stakeholders, for example, to choose the box insulation and the PCM mass according to the product to transport, duration and ambient temperature during the supply chain.

It is to be emphasized that certain experimental data presented in this article were used for a thermal model development based on the zonal approach. This model takes into account conduction, convection and radiation inside an insulated box (Leungtongkum et al., 2023b).

2. Material and methods

The material and methods described in detail in Leungtongkum et al. (2023a) are presented succinctly below.

2.1 Experimental setup

For thermal study, the box is a 45-L commercialized multilayer insulated box (Manutan SA, Gonesse, France). In fact, commercialized boxes are available in various sizes (from less than 5 L to more than 300 L). For meat, a highly perishable food, the boxes generally do not exceed 50 L. To be close to real situations, we chose a 45-L box in our study. For airflow study, the box has the same dimensions and wall structure as the one for thermal study, but two side walls are replaced by triple-glazed windows (3 glass panes each with a thickness of 4 mm, 2 argon-filled 10-mm gaps) to allow the entrance of laser sheet and the image capture by a camera. The overall heat transfer coefficient of the walls of these two boxes is almost the same (0.89 $W \cdot m^{-2} \cdot K^{-1}$).

The PCM container, made of polypropylene (3.5-mm thickness), had external dimensions 460 mm x 280 mm x 50 mm and was filled with 3.5 kg of tap water (melting point ~ 0°C). The thermophysical properties of PCM (water in this study), in both liquid and solid state along with its enthalpy of melting is shown in Table 1. Since the form of food is diverse, Tylose packs are used as test product (dimensions of a pack 200 mm x 100 mm x 50 mm) as that used in standard tests for thermal performance of cold equipment. The physical properties of this test product are close to the ones of meat (Table 1). This configuration (compact load with air gaps between load and box walls) was studied by several authors (Ohkawara et al., 2012; Zhao et al., 2019).

The box can be placed horizontally (*AR*, height/width ≈ 1) or vertically (*AR* ≈ 1.7), making it possible to study the effect of the aspect ratio on heat transfer and the airflow pattern. The effect of the air space underneath the product was studied by placing the test product on a perforated support made of galvanized steel (length x width x height = 350 x 150 x 20 mm and 150 x 150 x 20 mm for a horizontal and a vertical box, respectively). An example of experimental setup for a horizontal box with PCM on a side wall is shown in Figure 1.

2.2 Thermal study

To assure the homogeneous initial PCM temperature, a PCM slab was placed horizontally in a freezer set at a temperature of -2°C for at least 48 h before each experiment. To assure the homogeneous initial product temperature, sixteen packs of test product were placed in a polystyrene box and stored in a domestic refrigerator set at a temperature of 4°C or 10°C for at least 24 h before each experiment. In this manner, the product temperature is not influenced by the air temperature fluctuation due to "on" and "off" compressor working cycles.

Temperatures of PCM, air, and test product in the loaded box (Figure 1) were measured at 35 positions located in the middle plane (x = 250 mm) every 30 s from 400 min. to 600 min. after closing the box to assure the stabilization of temperature during the measurement. The temperature contour map was drawn by MATLAB by interpolation from 30 measured points. More detail on temperature measurements can be found in Leungtongkum et al. (2023a).

It is to be emphasized that the T-type thermocouples were previously calibrated at -10°C, 0°C, 10°C, 20°C and 30°C and allowed the measurement precision of ± 0.2°C.

Table 2 describes the experimental conditions (cf. the detailed description in Section 2.4). Conditions 1, 2, 9 and 10 were done twice to verify the repeatability of the results. These conditions are notified by "*" in Table 2. Since the result repeatability was observed in these conditions (standard deviation ~ 0.2°C), the other ones reported in this Table were done only once allowing a large number of experimental conditions to be fulfilled.

2.3. Airflow study

Non-intrusive air velocity measurements were achieved by PIV (Particle Image Velocimetry). The PIV device is constituted of three components: a double-pulsed Nd:YLF laser (527 nm wavelength, 10 mJ pulse energy), a high-speed 12-bit CMOS video camera (Photron, FASTCAM SA3; 1024 × 1024 pixels in resolution) fitted with a lens (Sigma; 105 mm, f/1:2.8) and a programmable timing unit (PTU-X) to ensure synchronization of the laser and the camera. Visualization of the airflow pattern is possible by the scattering of smoke particles during laser pulses. Oil-based particles (mean diameter 0.3 μm) were generated using a smoke machine (Antari, F-80Z). Based on our calibration, the image size was 115.5 mm x 115.5 mm. The positions of the measured windows partially overlapped with the neighboring one using the displacement system. Finally, the air velocity field over the whole area of the plane could be developed.

For each measured window, 500 pairs of images were recorded every 20 ms with a time interval of 900 μs between two images of the same pair (between two laser pulses) with the total measurement duration of 10 s. After capturing all the images, instantaneous airflow vectors were calculated using a cross-correlation method with a multi-pass correlation algorithm (Raffel et al., 2007). The distance between two vectors was around 0.9 mm in both horizontal and vertical directions. After 500 instantaneous vector fields had been attained, the mean velocity field of each measured window was calculated. More detail on PIV system, image acquisition, image post-processing and experimental protocol can be found in Leungtongkum et al. (2023a).

2.4 Experimental conditions

Table 2 summarizes the investigated experimental conditions: position of PCM, aspect ratio of the box, ambient temperature, initial test product temperatures and its position. The pictograms were introduced for further reference. The studied conditions (except PCM position) are new in comparison to the ones presented in Leungtongkum et al. (2023a).

3. Results and discussions

In addition to the results presented in our previous work (Leungtongkum et al., 2023a), this article focuses on the influence of box designing and operating parameters on temperature and air velocity fields: box aspect ratio and PCM position (Figure 2), external and initial product temperatures (Figure 3), space beneath the test product (Figure 4). These influences on the average, min and max temperatures of product core/surface and air at stable condition are summarized in Table 3. To complete the data at stable condition, the time-temperature evolutions at different positions are presented in Figure 5, the analysis of the time to reach stable condition (thermal time constant) quantitatively shows the importance of heat fluxes by conduction and convection. The experimental results shown in Figure 6 show the effect of the amount of PCM on product temperature. Finally, simple equations are proposed to predict the maximum storage time in function of box insulation, PCM mass, melting point, product mass, ambient temperature.

3.1 Effect of the aspect ratio

Figure 2 shows the airflow pattern and the temperature field on the middle plane of horizontal and vertical loaded boxes with PCM on the right side. The absence of air velocity in the gap between the test product and PCM of the horizontal box can be explained by the impossibility of laser sheet projection in this zone, thus, no PIV measurement. The same reason explains the absence of air velocity in the gap below the test product of the vertical box.

When PCM was on the side (Figures 2a and 2c), air flows downwards close to PCM and flows upwards close to the opposite vertical wall. In the gap between the test product and the box wall (left side), the upward maximal velocity was similar in both cases (~ 0.11 $m \cdot s^{-1}$, with an uncertainty of 3 x 10^{-3} $m \cdot s^{-1}$). Comparison is not possible in the gap between the PCM and the test product. However, in the vertical box, the maximal downward velocity (0.13 $m \cdot s^{-1}$, with an uncertainty of 3 x 10^{-3} $m \cdot s^{-1}$) was higher than the maximal upward velocity (0.11 $m \cdot s^{-1}$, with an uncertainty of 3 x 10^{-3} $m \cdot s^{-1}$). This is because downward flow occurs only along the PCM, whereas upward flow occurs not only along the opposite wall but also along the two other vertical box walls (results not shown).

Regarding the temperature field (Figures 2a' and 2c'), increasing the height of the box did not change the coldest and warmest positions. The coldest spot was located at the bottom close to the PCM surface and the warmest spot was at the top close to the opposite side wall.

Table 3 summarizes the average temperatures observed between 400 and 600 min. considered as a stable period. In the pictograms, the cold/warm spot locations for air and the product are shown. This table distinguishes the temperature of air, of the product surface and of the product core in terms of average, maximum and minimum values. In the following section, we will focus on the average product core value, $T_{pc,\ ave}$ and the maximum product temperature (core or surface), $T_{p,\ max}$, because of the importance for product quality and the sanitary risk (on the average and for the highest temperature location). Indeed, the minimum product temperature was always positive (no freezing risk) since PCM was initially at a temperature of -2°C and melted near 0°C. To complement these findings, we will also consider the air temperature heterogeneity: $\Delta T_{air} = T_{air,\ max} - T_{air,\ min}$. Since the standard deviation (SD) between replicates for average product (core or surface, 4 positions each) temperatures is around 0.2°C (see Table 3), we should consider that a difference of less than about 0.5°C does not exert a significant impact on product quality evolution.

Increasing the height of the box significantly led to higher product temperatures and greater air temperature heterogeneity:

<u>Horizontal box:</u> $T_{pc,\ ave}$ = 5.8°C, $T_{p,\ max}$ = 7.7°C, ΔT_{air} = 6.0°C, SD of T_{air} = 2.2°C

<u>Vertical box:</u> $T_{pc,\ ave}$ = 7.8°C, $T_{p,\ max}$ = 9.9°C, ΔT_{air} = 7.5°C, SD of T_{air} = 3.0°C

A higher aspect ratio (height/width) leads to larger temperature differences between the top and the bottom. Thus, it is recommended to limit the height of insulated boxes. In fact, increasing the height should increase convective heat transfer between PCM and air (according to Nu-Ra correlations) but the air pathway along the box walls is longer and thermal stratification is stronger. Finally, under conditions close to ours, these different phenomena lead to higher average temperature and temperature heterogeneity for higher aspect ratio.

3.2 Effect of the PCM position

The effect of PCM position on temperature and air velocity fields of a horizontal box are shown in Figure 2. For PCM at top, upward flow was observed near the left box wall and also near the top of test product but only a very weak downward flow (dashed arrow A in Figure 2b) was noticed in the left gap. In fact, flow was asymmetric: under the PCM, cold air flows preferentially towards the right gap where downward flow certainly dominates, whereas upward flow dominates in the left gap.

The temperature distribution on the middle plane (Figure 2b') also shows a dissymmetry of air and product temperatures. Air was at a temperature of around 5.2°C in the right gap and around 6.6°C in the left gap. This confirms the hypothesis of asymmetric airflow.

Placing PCM at the top allowed lower average temperature and lower air temperature heterogeneity:

PCM on the side: $T_{pc,\,ave}$ = 5.8°C, $T_{p,\,max}$ = 7.7°C, ΔT_{air} = 6.0°C, SD of T_{air} = 2.2°C

PCM at the top: $T_{pc,\,ave}$ = 5.4°C, $T_{p,\,max}$ = 6.6°C, ΔT_{air} = 2.5°C, SD of T_{air} = 1.1°C

Hence, placing PCM at the top is more appropriate for food transport and this configuration was used for further study of the influence of ambient and initial test product temperatures.

3.3 Effect of ambient temperature

Figure 3 presents the temperature field of the loaded box with a 20-mm air gap underneath and PCM at the top under ambient temperatures of 10°C (Figure 3a), 20°C (Figure 3b) and 30°C (Figure 3c). To compare the effect of different ambient temperatures on measured temperatures, the dimensionless temperature T^* was defined (Equation 1).

$$T^* = \frac{T - T_m}{T_{amb} - T_m} \qquad (1)$$

where T is the average value of the temperatures measured between 400 min. and 600 min.

Logically, increasing ambient temperature led to a higher product temperature and greater air temperature heterogeneity:

T_{amb} = 10°C: $T_{pc,\,ave}$ = 4.3°C ($T^*_{pc,\,ave}$ = 0.43), $T_{p,\,max}$ = 5.2°C, ΔT_{air} = 1.7°C, SD of T_{air} = 0.5°C

T_{amb} = 20°C: $T_{pc,\,ave}$ = 5.4°C ($T^*_{pc,\,ave}$ = 0.27), $T_{p,\,max}$ = 6.6°C, ΔT_{air} = 2.5°C, SD of T_{air} = 1.1°C

$\underline{T_{amb} = 30°C:}$ $T_{pc,\,ave}$ = 7.2°C ($T^*_{pc,\,ave}$ = 0.24), $T_{p,\,max}$ = 9.1°C, ΔT_{air} = 4.8°C, SD of T_{air} = 1.6°C

The positions of the coldest and warmest spots were the same for all ambient temperatures. One could expect that in terms of dimensionless temperature, the results would be the same, but this is not the case when applied to the average core temperature (T^* varying between 0.43 and 0.24). This can be due to the non-linearity of heat fluxes versus temperature difference in free convection: fluid flow and consequently the convective heat transfer coefficient which depends on the temperature difference. This was effectively observed with more noticeable downward airflow at an ambient temperature of 30°C (result not shown). This can also be due to the influence of the initial product temperature which is different in dimensionless terms for the three ambient temperatures (thermal inertia effect). Thus, a simple linear extrapolation cannot be applied for different ambient temperatures. For example, a 50% increase in the difference between the ambient temperature and the PCM melting temperature does not necessarily lead to a 50% higher product temperature. Similar results were obtained for PCM on the side (see Table 3, conditions 1 and 4). Physical-based models, e.g. zonal model or CFD, could be used to analyze the effect of ambient temperature on temperature heterogeneity and temperature evolution.

3.4 Effect of the initial test product temperature

Figure 3d presents the temperature field for an initial test product temperature of 10°C and PCM at the top under ambient conditions of 20°C. By comparing Figures 3b and 3d, it was observed that a higher initial test product temperature led to a higher product temperature:

$\underline{T_{pc,\,ini} = 4°C:}$ $T_{pc,\,ave}$ = 5.4°C ($T^*_{pc,\,ave}$ = 0.27), $T_{p,\,max}$ = 6.6°C, ΔT_{air} = 2.5°C, SD of T_{air} = 1.1°C

$\underline{T_{pc,\,ini} = 10°C:}$ $T_{pc,\,ave}$ = 8.0°C ($T^*_{pc,\,ave}$ = 0.40), $T_{p,\,max}$ = 9.2°C, ΔT_{air} = 2.8°C, SD of T_{air} = 0.9°C

Theoretically, the same results would be expected under steady state conditions, whatever the initial test product temperature if the same ambient temperature and PCM melting point are applied. This means that even after 8 h (on an averaged basis between 400 and 600 min.), steady state was not reached. This is highlighted in Section 3.6.

Similar results were obtained for PCM on the side (see Table 3, conditions 1 and 7). Concerning application aspects, placing a load with a high initial temperature in packaging is not recommended for food transport because PCM should only serve to maintain the product temperature, not to cool it.

3.5 Effect of a space beneath the test product

Figure 4 illustrates the air velocity field for the box with PCM at the top and on the side with a 20-mm gap underneath the test product (Figure 4a and Figure 4c) and without a gap (Figure 4b and Figure 4d). This gap is expected to ensure better air circulation and avoid direct heat conduction from the bottom wall to the product.

When PCM was at the top (Figures 4a and 4b), the airflow pattern was quite similar with and without gap. From Table 3, for PCM at the top, it appears that the influence of gap beneath the test product on the product temperature is not significant.

<u>With a 20-mm gap:</u> $T_{pc,\,ave}$ = 5.4°C, $T_{p,\,max}$ = 6.6°C, ΔT_{air} = 2.5°C, SD of T_{air} = 1.1°C

<u>Without gap:</u> $T_{pc,\,ave}$ = 5.6°C, $T_{p,\,max}$ = 7.2°C, ΔT_{air} = 2.6°C, SD of T_{air} = 1.0°C

When PCM was on the side (Figure 4c and 4d), the maximum air velocity was slightly higher with the gap (0.13 $m \cdot s^{-1}$, with an uncertainty of 3 x 10^{-3} $m \cdot s^{-1}$ and 0.10 m s^{-1}, with an uncertainty of 9 x 10^{-3} $m \cdot s^{-1}$ in the box with 20-mm gap underneath and without a gap, respectively). In spite that the presence of gap led to better air circulation, the influence on product temperature was not obvious. From Table 3, for PCM on the side:

<u>With a 20-mm gap:</u> $T_{pc,\,ave}$ = 5.8°C, $T_{p,\,max}$ = 7.7°C, ΔT_{air} = 6.0°C, SD of T_{air} = 2.2°C

<u>Without gap:</u> $T_{pc,\,ave}$ = 5.8°C, $T_{p,\,max}$ = 7.5°C, ΔT_{air} = 7.3°C, SD of T_{air} = 2.5°C

Since the presence of gap has insignificant influence on product temperature, it is more practical to load the product directly onto the bottom of the box without providing a gap.

3.6 Temperature evolution

Figure 5 presents the temperature evolution at several positions in a loaded horizontal box with PCM on the side after the lid was closed. The internal wall (TC1), internal air (TC2, TC5 and TC8) and PCM surface temperatures (TC9) decreased rapidly over a period of around 60 min. before gradually increasing, while the surface and core temperatures of the test product (TC3, TC4, TC6 and TC7) increased slowly over a period of 1100 min. (18 h).

The difference in temperature evolution of the walls of the box and the test product can be explained by their thermal inertia, diffusivity and convective heat exchange with air. The Biot number (*Bi*) was used to compare the effect of the internal and external thermal resistance of these materials, as defined in Equation. 2:

$$Bi = \frac{hL}{\lambda} \qquad (2)$$

where L is the characteristic length represented by the thickness of the inner polypropylene layer (3.5 mm) for a wall of the box (considering that heat exchanged only with one side) and by the half thickness of the test product (100 mm). Due to natural convection inside the box, the order of magnitude of the heat transfer coefficient is approximately 5 $W{\cdot}m^{-2}{\cdot}K^{-1}$.

Consequently, the Biot number is 0.146 for polypropylene and 0.98 for the test product. Hence, the thermal resistance of the internal wall could be neglected, while that of the test product is of the same order of magnitude as the external thermal resistance.

The thermal time constant related to conduction can be estimated by Equation. 3 (Bergman et al., 2011).

$$\tau_{conduction} = \frac{\rho C_p L^2}{\lambda} \quad (3)$$

Similarly, the thermal time constant related to convection can be estimated by Equation. 4 (Bergman et al., 2011).

$$\tau_{convection} = \frac{\rho C_p L}{h} \quad (4)$$

For the internal wall, the thermal time constants for conduction and convection are 179 s (3 min.) and 1230 s (20 min.), respectively. It can be concluded that the delay in temperature evolution of the internal walls was mainly caused by convection between adjacent air and the walls.

For the test product, the thermal time constants of conduction and convection are 70800 s (> 19 h) and 72200 s (> 20 h), respectively. Thus, both heat conduction and convection play an important role in the temperature evolution, and this explains the temperature difference between the core, the surface of test product and the adjacent air.

The thermal time constants of the test product are much longer than those of the internal wall and this results in a different rate of temperature evolution.

According to Figure 5, the internal temperature of PCM (TC10) increased after 800 min. (~13 h) indicating that PCM was melted. The temperature of the other components thus increased. In view of the thermal time constant for the product, PCM is melted before the product reaches thermal equilibrium, so there was no steady state in this condition. One could consider a hypothetical equilibrium temperature which would be reached after a long period by assuming that PCM is still at the melting temperature everywhere. Roughly, for horizontal boxes, for PCM either at the top or on the side:

<u>$T_{pc, ini}$ = 4°C:</u> after 8 h, $T_{pc, ave}$ is at around 5.5°C and the temperature is still rising

<u>$T_{pc, ini}$ = 10°C:</u> after 8 h, $T_{pc, ave}$ is at around 8.5°C and it is still decreasing

Therefore, the equilibrium temperature should be around 7°C.

In practice, to be able to compare the performances of insulated boxes equipped with PCM, the experiments should be carried out under the same loading conditions (mass and initial temperature), ambient temperature and duration of temperature measurement.

3.7 Effect of the amount of PCM on the test product temperature evolution and maximum storage time

This section describes a comparison of the experimental test product core temperature evolution (average of four measurements at different locations) for 3 amounts of PCM: 0 kg, 1.7 kg (about 10% of the product mass), and 3.5 kg (about 20% of the product mass) (Figure 6a). This experiment was undertaken for PCM located on a sidewall of a horizontal box loaded with the test product at an initial temperature of 4°C and 20°C ambient temperature. The higher amount of PCM lowered the rate of temperature increase. For example, during the first 2 h, this rate was 1.13°C·h^{-1}, 0.58°C·h^{-1} and 0.34°C·h^{-1}, for 0 kg, 1.7 kg and 3.5 kg of PCM, respectively.

Figure 6b presents the relationship between the maximum product storage time (t_{max}) and the amount of PCM. This maximum storage time is defined as the duration during which the product remains below $T_{p,max}$ = 8°C, which is the maximum temperature value for the storage of certain chilled foods. The higher the amount of PCM, the higher the maximum storage time: 370 min. (for 0 kg), 944 min. (for 1.7 kg) and 1373 min. (for 3.5 kg). The results obtained in terms of product temperature evolution and maximum storage time confirm the benefit of PCM for food preservation as reported by Zhao et al. (2019) for strawberries. These authors showed that the use of PCM allowed less weight loss and greater product firmness in comparison with the case where PCM was not used.

To determine approximately the maximum storage time as a function of the amount of PCM, the following heat balance equation can be used:

$$m_p C_{p,p}\left(T_{p,max} - T_{p,ini}\right) + m_{pcm} L_f = UA\left(T_{amb} - \frac{T_{p,ini} + T_{p,max}}{2}\right) t_{max} \qquad (5)$$

where U is the overall heat transfer coefficient of the box [W·m^{-2}·K^{-1}]

and A is the exchange area [m²]

The overall heat transfer coefficient of the box can be related to the thicknesses (e_k) and conductivities (λ_k) of the box wall materials (of index k) as shown in Equation 6 (assuming negligible convective heat transfer resistances).

$$\text{Thus, } U = \frac{1}{\sum_k \frac{e_k}{\lambda_k}} \qquad (6)$$

Equation 5 assumes that PCM is completely melted when $T_{p,max}$ is reached and that the internal temperature is close to the average test product temperature.

Based on these assumptions, Equation 5 becomes:

$$t_{max} = t_{max,0}\left(1 + \alpha \frac{m_{pcm}}{m_p}\right) \qquad (7)$$

where $t_{max,0}$ is the maximum storage time of the box without PCM defined as

$$t_{max,0} = \frac{m_p C_{p,p}(T_{p,max} - T_{p,ini})}{UA\left(T_{amb} - \frac{T_{p,ini} + T_{p,max}}{2}\right)} \qquad [s]$$

$$\text{and} \quad \alpha = \frac{L_f}{C_{p,p}(T_{p,max} - T_{p,ini})} \qquad [-]$$

This indicates a linear relationship between the maximum storage time and the amount of PCM as shown in Figure 6b.

In practice, for all types of boxes, it is suggested that this type of experiment should be conducted, at a fixed ambient temperature, without and with a given amount of PCM to determine $t_{max,0}$ and α. The influence of other parameters could be approximated according to

Equations 5 and 7. For example, it is expected that the maximum storage time is inversely proportional to the difference between the ambient temperature (T_{amb}) and the internal temperature considered as the average test product temperature ($\frac{T_{p,ini} + T_{p,max}}{2}$).

3.8 Expected influence of insulation on temperature level and heterogeneity

The present study considered only one insulation configuration. This section aims to predict the effect of changing the insulation by using a basic approach. This effect is the determining factor for the temperature distribution in insulated boxes equipped with PCM (Paquette et al., 2017). To illustrate the influence of the box insulation, the analysis presented below concerns the box with PCM on the side where a higher temperature level and greater heterogeneity were observed.

As a first approach, the steady state mean temperature in the box (T_{mean}) could be obtained from the following energy balance (Equation 8):

$$A_c h_c (T_{mean} - T_m) = A_w U (T_{amb} - T_{mean}) \qquad (8)$$

where A_c and A_w are the surface area of warm (insulated) and cold (PCM) walls [m^2],

h_c is the heat transfer coefficients between product and PCM surface [W·m^{-2}·K^{-1}],

U is the overall heat transfer coefficient between ambient and product surface through box insulation [W·m^{-2}·K^{-1}] and

T_m and T_{amb} are the melting temperature of the PCM and the external temperature, respectively [°C].

When the box is horizontal, in our case $\beta = (A_w U)/(A_c h_c) \approx 0.54$ with $T_m = 0$°C, $T_{amb} = 20$°C and $T_{mean} \approx 7$°C. Since $A_w/A_c = 4.3$ and $h_c/U \approx 8$; therefore, if insulation is improved by 30%, (i.e., U divided by 1.3), the mean temperature should decrease from 7°C to 5.9°C.

To obtain an estimation of temperature heterogeneity, it can be assumed that air flows, with a mass flowrate $\dot{m}$, first along the PCM, where its temperature decreases to T_{min}, then along the warm walls, where the temperature rises to T_{max}. The following equations characterize these heat exchange phenomena (Equations 9 and 10):

$$T_{air,min} - T_m = \alpha_c\left(T_{air,max} - T_m\right) \qquad (9)$$

where $$\alpha_c = exp\left(-\frac{A_c h_c}{\dot{m}C_{p,air}}\right)$$

$$T_{amb} - T_{air,max} = \alpha_w\left(T_{amb} - T_{air,min}\right) \qquad (10)$$

where $$\alpha_w = exp\left(-\frac{A_w U}{\dot{m}C_{p,air}}\right) = {\alpha_c}^{\beta}$$

Therefore; $$T_{air,max} - T_{air,min} = \frac{(1-\alpha_c)(1-\alpha_w)(T_{amb} - T_m)}{(1-\alpha_c\alpha_w)} \qquad (11)$$

For the academic case of a square cavity with one vertical cold wall (T_c), one vertical warm wall (T_w) and adiabatic horizontal walls, Raithby & Hollands (1998) found that $T_{air,max} - T_{air,min} \approx 0.5(T_w - T_c)$ for the cavity with a low aspect ratio (AR < 40) which is often the case of insulated boxes (T_w and T_c are the temperature of warm wall and cold wall, respectively). If our basic approach is applied to this case, it can be estimated that $\alpha_c \approx 1/3$.

In our case ($\beta \approx 0.54$), it was calculated that $T_{air,max} - T_{air,min} \approx 7.4$°C which is comparable to the observed values. If insulation is improved by 30% for example (β divided by 1.3), the temperature heterogeneity should decrease from 7.4°C to 6.1°C.

This basic approach does not take into account the interaction with the test product especially during the unsteady period, radiation, complex flow etc., but it allows a rough estimation of the influence of insulation. It also highlights the influence of the air mass flowrate ($\dot{m}$) and the heat transfer (h_c) along the PCM on the temperature level and heterogeneity.

4. Conclusion and perspectives

This study investigated airflow and temperature fields inside an insulated box equipped with PCM loaded with test product (Tylose slabs). PCM position significantly affected airflow patterns, air temperature profile, product temperature homogeneity, and average product temperature. When PCM was on a sidewall, the coldest position was at the bottom, close to the PCM surface, and the warmest one was at the top close to the opposite vertical wall. When PCM was at the top, the lowest product temperature was located at the top, while the highest one was at the bottom, and slightly lower air and product temperatures were observed. Increasing the box aspect ratio (higher box) led to a higher product temperature and greater temperature heterogeneity (at least for PCM on the side). The non-linear correlation between ambient temperature and product temperature can be explained by the non-linearity of free convection and the product thermal inertia. An insignificant influence of the initial product temperature on the airflow pattern and air velocity profile was observed. The presence and absence of a space underneath the product led to similar temperatures, despite the difference in airflow pattern in the case of PCM on the side.

It is recommended that the PCM should be placed at the top of the box in order to reduce temperature stratification. This configuration has been previously investigated in an empty cavity and this work confirms, by experiment, that it can be applied for the loaded cavity as well. The box should not be too high to avoid a high temperature and large temperature heterogeneity. The effect of aspect ratio is complex as higher boxes allow higher convective heat transfer and also higher thermal stratification. Thus, CFD model is suggested to analyze in detail the influence of aspect ratio on temperature distribution. To maintain the product temperature along a supply chain, PCM could be placed on all walls (top, bottom, sidewalls); however, the available volume would be significantly reduced and the logistic cost per kg of product would be higher. Our study demonstrates that it is possible to place PCM only at one wall (top or side) if an appropriate PCM mass is used. This mass depends on the ambient temperature in the supply chain, which directly impacts airflow and product temperature. Hence, the ambient temperature is an important factor for the system design, i.e., box wall material, PCM type and mass. However, linear extrapolation from one ambient to another is not recommended because of non-linear behavior, thus physical based models taking natural convection into account should be used to analyze the impact of ambient temperature on product temperature in an insulated box with PCM. Loading a product at a high temperature should be avoided since it takes more than 10 hours to cool it down according to its high thermal inertia. Adding a 20-mm air space beneath the test product neither reduces the test product temperature nor increases homogeneity although this gap allows slightly better air circulation. Future studies are required to determine the influence of the other air gaps: between PCM and load, between lateral and top walls and load. The use of PCM can delay the internal temperature evolution and the amount of PCM linearly correlates with the maximum storage time of the insulated box. The influence of other parameters like the amount of product and the emissivity of box walls will be studied.

The experimental velocity and temperature fields obtained in different conditions can further be used to validate CFD models. They should confirm that when PCM is at top, although the configuration is symmetric, the velocity and temperature fields can be asymmetric. In practice, there are many other possible box designs and operating conditions and the interactions between the different factors are complex. Thus, numerical models are necessary for investigating the influence of these factors on temperature distribution and evolution in a wide variety of configurations (e.g., smaller/larger boxes, improved insulation). The experimental results presented in the present article can contribute to validate these models.

Acknowledgement

King Mongkut's Institute of Technology Ladkrabang, Thailand (contract no. KREF156402), French Embassy in Thailand, and the National Research Institute for Agriculture, Food and Environment, France are gratefully acknowledged for their financial support. The authors would also like to thank the Royal Thai Government Scholarship and Chulalongkorn University, Bangkok, Thailand for T. Leungtongkum's PhD scholarship. This research did not receive any specific grant from funding agencies in the public, commercial, or not-for-profit sectors. Thanks to LaVision for PIV technical support.

References

Ataei-Dadavi, I., Chakkingal, M., Kenjeres, S., Kleijn, C. R., & Tummers, M. J. (2019). Flow and heat transfer measurements in natural convection in coarse-grained porous media. *International Journal of Heat and Mass Transfer*, *130*, 575–584. https://doi.org/10.1016/j.ijheatmasstransfer.2018.10.118

Bergman, T. L., Lavine, A. S., Incropera, F. P., & DeWitt, D. P. (2011). *Introduction to Heat Transfer*. John Wiley & Sons.

Burgess, S., Wang, X., Rahbari, A., & Hangi, M. (2022). Optimisation of a portable phase-change material (PCM) storage system for emerging cold-chain delivery applications. *Journal of Energy Storage*, *52*, 104855. https://doi.org/10.1016/j.est.2022.104855

Calati, M., Righetti, G., Zilio, C., Hooman, K., & Mancin, S. (2023). CFD analyses for the development of an innovative latent thermal energy storage for food transportation. *International Journal of Thermofluids*, *17*, 100301. https://doi.org/10.1016/j.ijft.2023.100301

Cengel, Y. A., & Ghajar, A. J. (2020). *Heat and Mass Transfer: Fundamentals & Applications*. McGraw-Hill Education.

Choi, C., Cho, H. W., Ha, M. Y., & Yoon, H. S. (2015). Effect of circular cylinder location on three-dimensional natural convection in a cubical enclosure. *Journal of Mechanical*

Science and Technology, *29*(3), 1307–1318. https://doi.org/10.1007/s12206-015-0246-3

Du, J., Nie, B., Zhang, Y., Du, Z., Wang, L., & Ding, Y. (2020). Cooling performance of a thermal energy storage-based portable box for cold chain applications. *Journal of Energy Storage*, *28*, 101238. https://doi.org/10.1016/j.est.2020.101238

Icier, F., & Ilicali, C. (2005). The use of tylose as a food analog in ohmic heating studies. *Journal of Food Engineering*, *69*(1), 67–77. https://doi.org/10.1016/j.jfoodeng.2004.07.011

Kacimi, A., & Labranque, G. (2019). Combination of vacuum insulation panels and phase change materials in temperature-controlled containers. *Proceedings of the 25th IIR International Congress of Refrigeration: Montréal, Canada, August 24-30, 2019.* https://doi.org/10.18462/iir.icr.2019.0163

Labihi, A., Aitlahbib, F., Chehouani, H., Benhamou, B., Ouikhalfan, M., Croitoru, C., & Nastase, I. (2017). Effect of phase change material wall on natural convection heat transfer inside an air filled enclosure. *Applied Thermal Engineering*, *126*, 305–314. https://doi.org/10.1016/j.applthermaleng.2017.07.112

Laguerre, O., Derens, E., & Flick, D. (2018). Modelling of fish refrigeration using flake ice. *International Journal of Refrigeration*, *85*, 97–108. https://doi.org/10.1016/j.ijrefrig.2017.09.014

Laguerre, O., & Flick, D. (2004). Heat transfer by natural convection in domestic refrigerators. *Journal of Food Engineering*, *62*(1), 79–88. https://doi.org/10.1016/S0260-8774(03)00173-0

Lee, S. H., Seo, Y. M., Yoon, H. S., & Ha, M. Y. (2016). Three-dimensional natural convection around an inner circular cylinder located in a cubic enclosure with sinusoidal thermal boundary condition. *International Journal of Heat and Mass Transfer*, *101*, 807–823. https://doi.org/10.1016/j.ijheatmasstransfer.2016.05.079

Leporini, M., Corvaro, F., Marchetti, B., Polonara, F., & Benucci, M. (2018). Experimental and numerical investigation of natural convection in tilted square cavity filled with air. *Experimental Thermal and Fluid Science*, *99*, 572–583. https://doi.org/10.1016/j.expthermflusci.2018.08.023

Leungtongkum, T., Flick, D., Hoang, H. M., Steven, D., Delahaye, A., & Laguerre, O. (2022). Insulated box and refrigerated equipment with PCM for food preservation: State of the art. *Journal of Food Engineering*, *317*, 110874. https://doi.org/10.1016/j.jfoodeng.2021.110874

Leungtongkum, T., Laguerre, O., Flick, D., Denis, A., Duret, S., & Chaomuang, N. (2023a). Experimental investigation of airflow and heat transfer by natural convection in an insulated box with a Phase Change Material using a Particle Image Velocimetry technique. *Journal of Food Engineering*, *336*, 111207. https://doi.org/10.1016/j.jfoodeng.2022.111207

Leungtongkum, T., Laguerre, O., & Flick, D. (2023b). Simplified heat transfer model for real-time temperature prediction in insulated boxes equipped with a phase change material. *International Journal of Refrigeration*, *149*, 286–298. https://doi.org/10.1016/j.ijrefrig.2023.02.009

Margeirsson, B., Pálsson, H., Popov, V., Gospavic, R., Arason, S., Sveinsdóttir, K., & Jónsson, M. þór. (2012). Numerical modelling of temperature fluctuations in superchilled fish loins packaged in expanded polystyrene and stored at dynamic temperature conditions. *International Journal of Refrigeration*, *35*(5), 1318–1326. https://doi.org/10.1016/j.ijrefrig.2012.03.016

Miroshnichenko, I. V., & Sheremet, M. A. (2018). Turbulent natural convection heat transfer in rectangular enclosures using experimental and numerical approaches: A review. *Renewable and Sustainable Energy Reviews*, *82*, 40–59. https://doi.org/10.1016/j.rser.2017.09.005

Moreno, S., Hinojosa, J. F., Hernández-López, I., & Xaman, J. (2020). Numerical and experimental study of heat transfer in a cubic cavity with a PCM in a vertical heated wall. *Applied Thermal Engineering*, *178*, 115647. https://doi.org/10.1016/j.applthermaleng.2020.115647

Ohkawara, H., Kitagawa, T., Fukushima, N., Ito, T., Sawa, Y., & Yoshimine, T. (2012). A Newly Developed Container for Safe, Easy, and Cost-effective Overnight Transportation of Tissues and Organs by Electrically Keeping Tissue or Organ Temperature at 3 to 6°C. *Transplantation Proceedings*, *44*(4), 855–858. https://doi.org/10.1016/j.transproceed.2012.02.023

Paquette, J.-C., Mercier, S., Marcos, B., & Morasse, S. (2017). Modeling the thermal performance of a multilayer box for the transportation of perishable food. *Food and Bioproducts Processing*, *105*, 77–85. https://doi.org/10.1016/j.fbp.2017.06.002

Raffel, M., Willert, C., Wereley, S., & Kompenhans, J. (2007). *Particle Image Velocimetry: A Practical Guide*. https://doi.org/10.1007/978-3-540-72308-0

Rahimi-Khoigani, S., Hamdami, N., & Dalvi-Isfahan, M. (2023). Application of an improved latent heat storage system in the food packaging. *Journal of Food Engineering*, *341*, 111351. https://doi.org/10.1016/j.jfoodeng.2022.111351

Raithby, G. D., & Hollands, K. G. T. (1998). Natural convection. In W. M. Rohsenow, J. P. Hartnett, & Y. I. Cho, *Handbook of Heat Transfer* (3rd ed). McGraw-Hill.

Rincón-Casado, A., Sánchez de la Flor, F. J., Chacón Vera, E., & Sánchez Ramos, J. (2017). New natural convection heat transfer correlations in enclosures for building performance simulation. *Engineering Applications of Computational Fluid Mechanics*, *11*(1), 340–356. https://doi.org/10.1080/19942060.2017.1300107

Xiaofeng, X., & Xuelai, Z. (2021). Simulation and experimental investigation of a multi-temperature insulation box with phase change materials for cold storage. *Journal of Food Engineering*, *292*, 110286. https://doi.org/10.1016/j.jfoodeng.2020.110286

Zhang, X., Su, G., Yu, J., Yao, Z., & He, F. (2015). PIV measurement and simulation of turbulent thermal free convection over a small heat source in a large enclosed cavity. *Building and Environment*, *90*, 105–113. https://doi.org/10.1016/j.buildenv.2015.03.015

Zhao, X., Xia, M., Wei, X., Xu, C., Luo, Z., & Mao, L. (2019). Consolidated cold and modified atmosphere package system for fresh strawberry supply chains. *LWT*, *109*, 207–215. https://doi.org/10.1016/j.lwt.2019.04.032

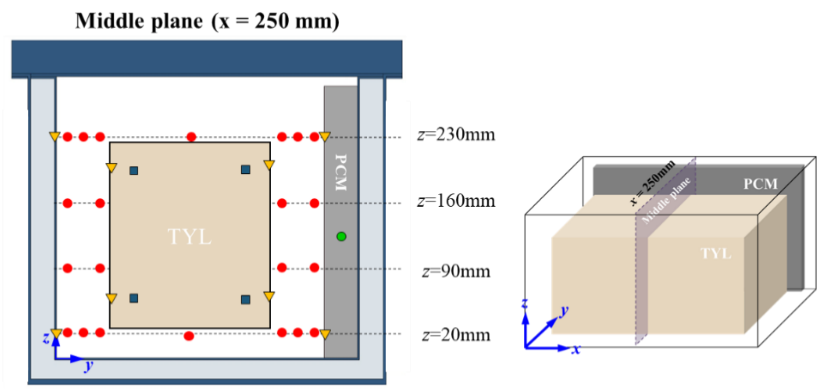

Figure 1: Experimental setup and thermocouple positions in the horizontal box with PCM on a side wall and loaded with the test product (Tylose, TYL). Note: Similar setup and measured positions were applied for the vertical box.

Air velocity field

Temperature field

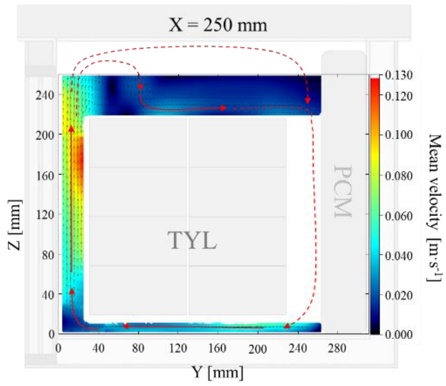

(a)

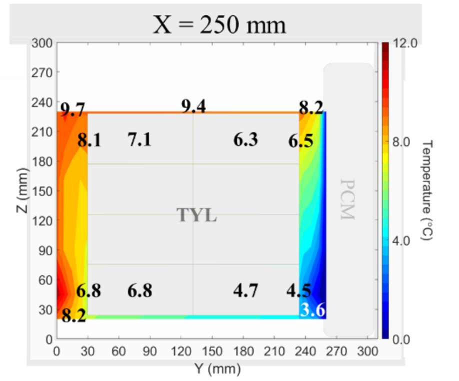

(a')

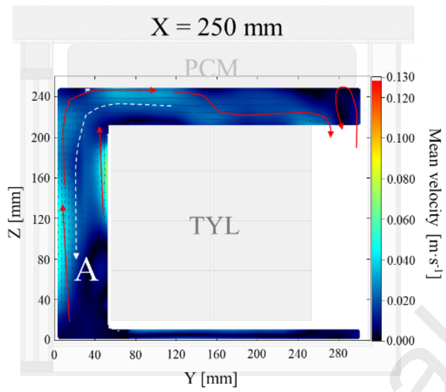

(b)

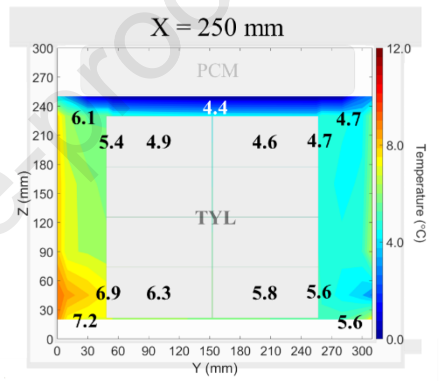

(b')

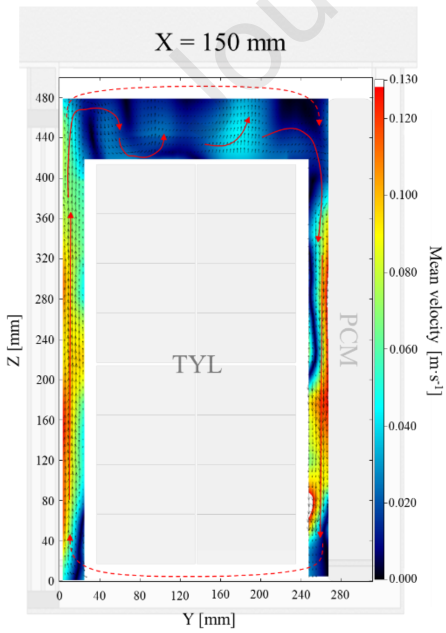

(c)

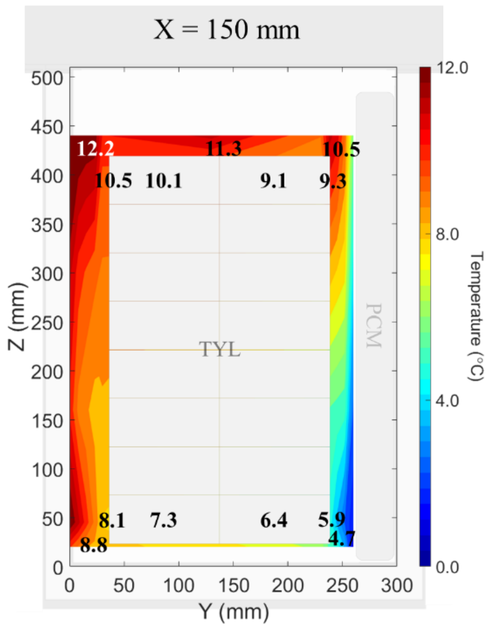

(c')

Figure 2: Measured air velocity field on the middle plane of a loaded box with (a) PCM on the side of the horizontal box; (b) PCM at the top of the horizontal box; and (c) PCM on the side of the vertical box. (a'), (b') and (c') are corresponding measured temperature fields (for one of the replications)

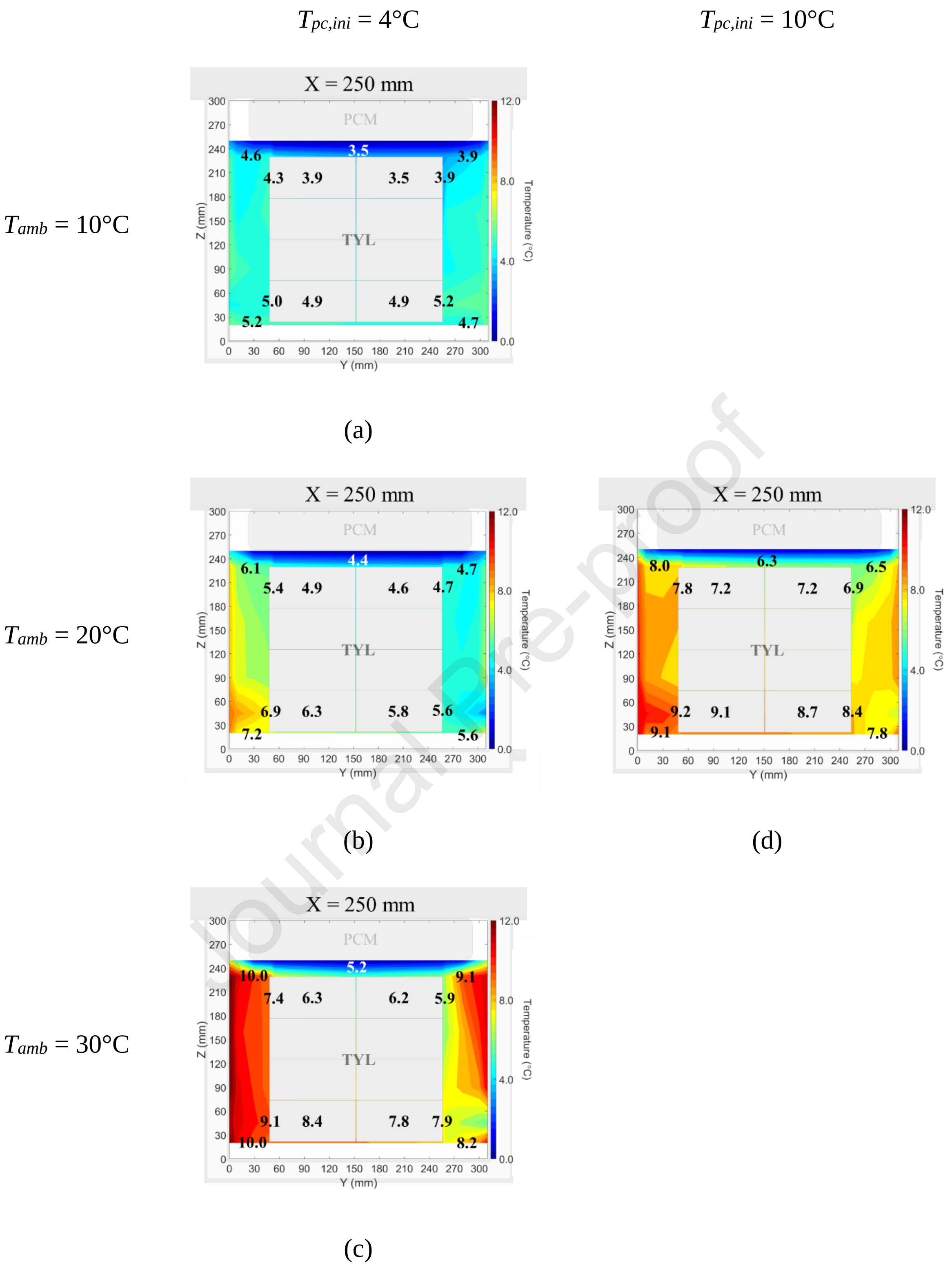

Figure 3: Measured temperature field on the middle plane of a loaded box with PCM at the top and a product initial temperature of 4°C under (a) 10°C ambient temperature; (b) 20°C ambient temperature; (c) 30°C ambient temperature; and (d) product initial temperature of 10°C under 20°C ambient temperature

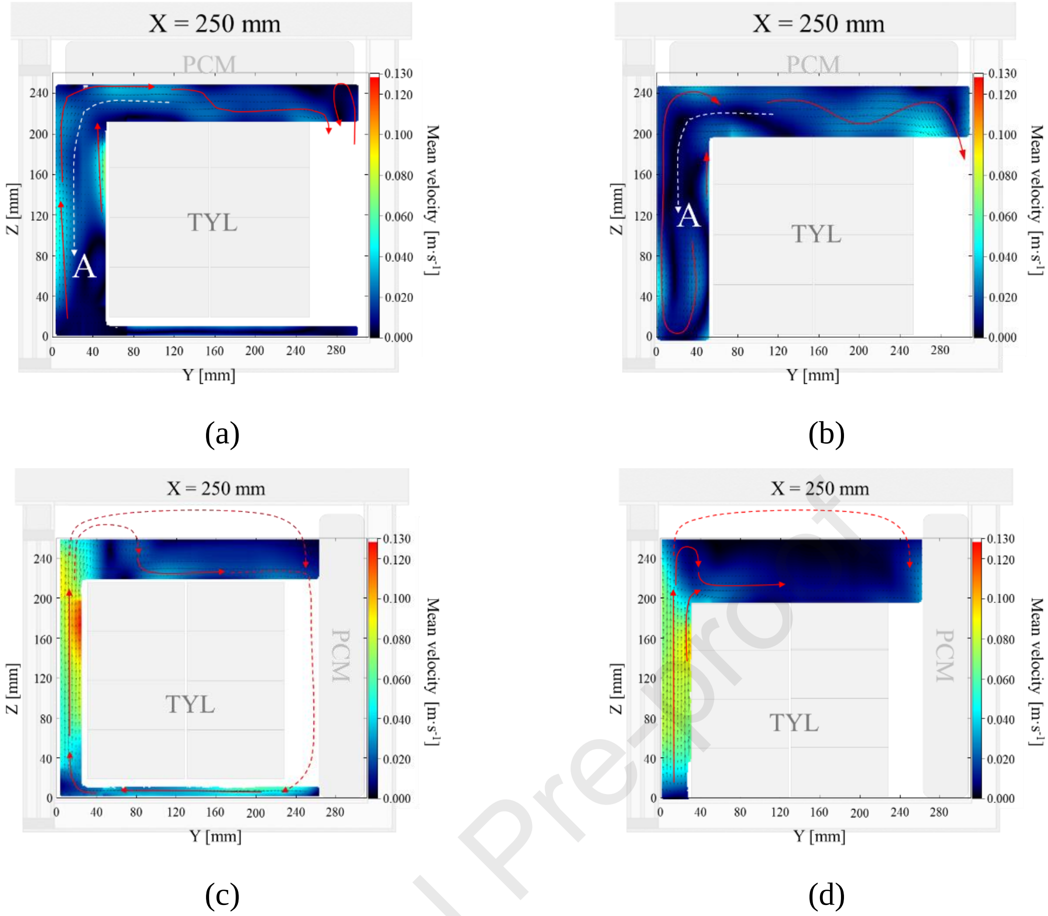

636 **Figure 4:** Measured air velocity field on the middle plane of a loaded box (a) PCM at the top,

637 20-mm gap underneath the test product, (b) PCM at the top, without gap, (c) PCM on the

638 side, 20-mm gap underneath the test product and (d) PCM on the side, without gap

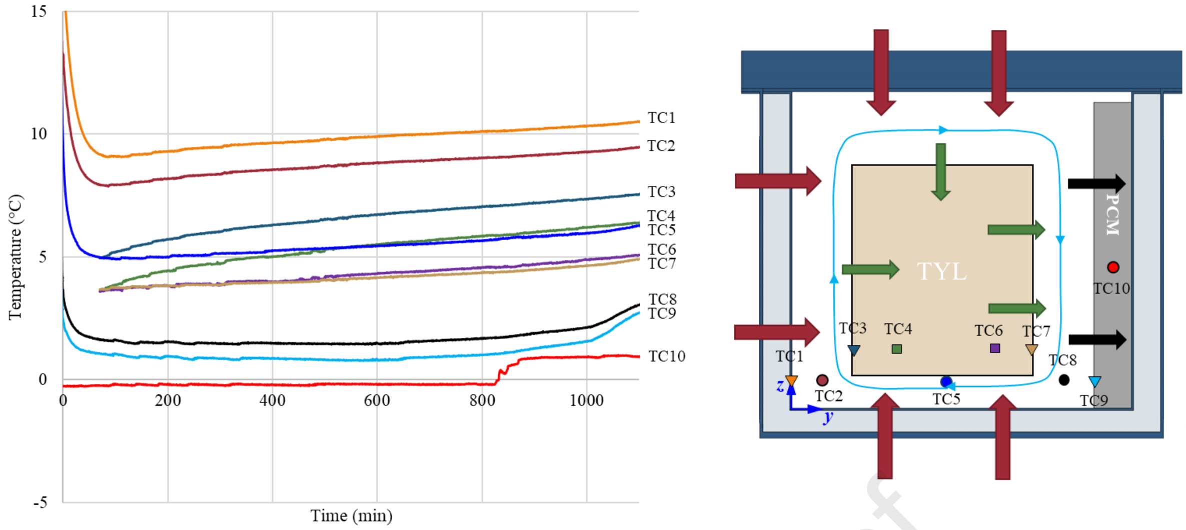

Figure 5: Temperature evolution at the bottom of the box during experiment No. 1 (ambient temperature = 20°C and initial test product temperature = 4°C) with heat flow (red arrows – from ambient, green arrows – between the internal air and the test product, and black arrows – from the internal air to the PCM). Airflow shown using blue arrows

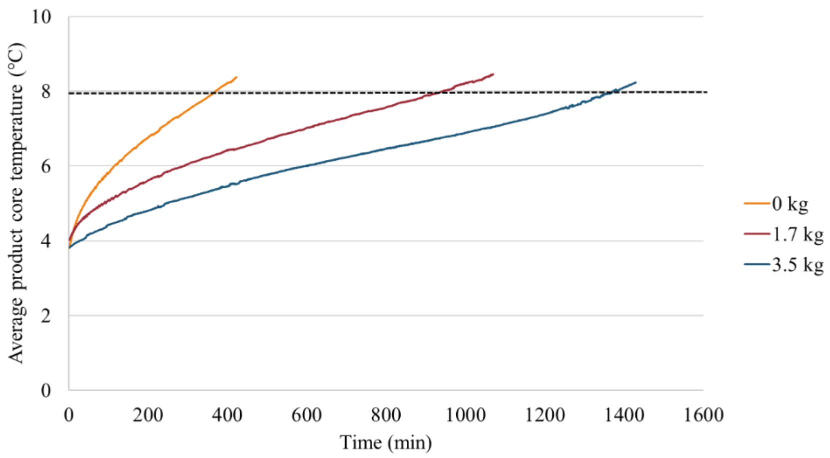

(a)

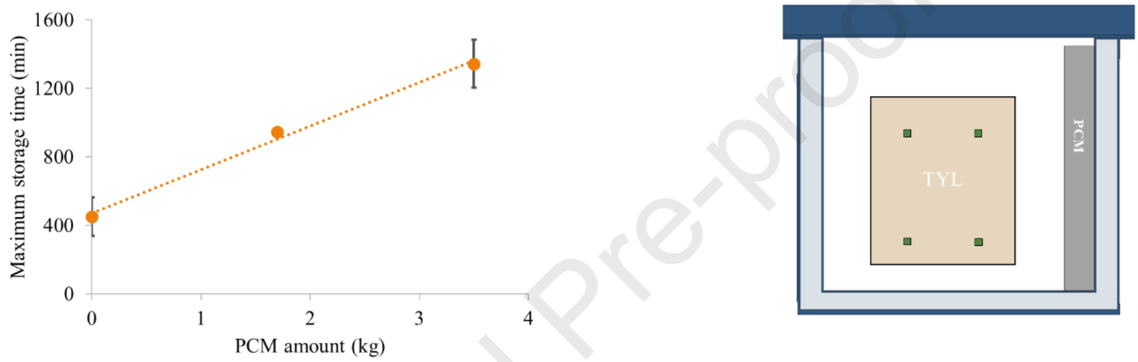

(b)

Figure 6: Effect of the amount of PCM on (a) test product core temperature evolution; and (b) maximum storage time, t_{max}. Error bars represent the standard deviation of 2 replications. The experiment was conducted under condition 4: loaded box with PCM on a sidewall with an ambient temperature of 20°C, 4°C initial product temperature, 20 mm gap beneath the test product (Tylose, TYL)

Table 1: Thermophysical properties of materials

Material	**ρ (kg·m^{-3})**	**C_p (J·kg^{-1}·K^{-1})**	**λ (W·m^{-1}·K^{-1})**	**Reference**
Liquid water	1000	4217	0.561	Cengel & Ghajar (2020)
*Ice	920	2040	1.880	Cengel & Ghajar (2020)
Test product (Tylose)	1070	3372	0.510	Icier & Ilicali (2005)

*Enthalpy of melting of ice (L_f) is 333700 J/kg with melting temperature (T_m) at 0°C

Table 2: Experimental conditions

Condition	1*	2*	3	4	5	6	7	8	9*	10*
	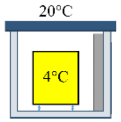	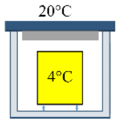	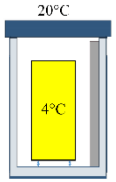	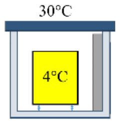	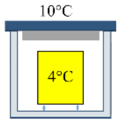	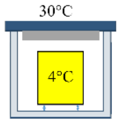	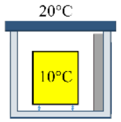	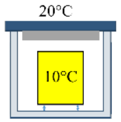	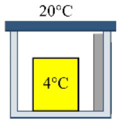	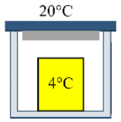
PCM position	Side	Top	Side	Side	Top	Top	Side	Top	Side	Top
Aspect ratio	~1	~1	1.7	~1	~1	~1	~1	~1	~1	~1
Ambient temperature (°C)	20	20	20	30	10	30	20	20	20	20
Initial test product temperature (°C)	4	4	4	4	4	4	10	10	4	4
Spacing beneath test product (mm)	20	20	20	20	20	20	20	20	0	0

* with two replications

Table 3: Test product core, surface and internal air temperatures for all experimental loaded conditions. Note: the reported values are the average of the temperatures measured between 400 min. and 600 min. considered as the stable thermal condition.

	Condition	***1	***2	3	4	5	6	7	8	***9	***10	**SD
	*Pictogram	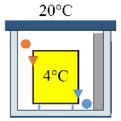	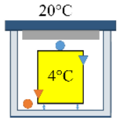	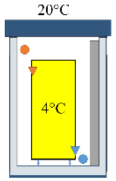	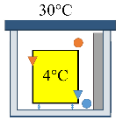	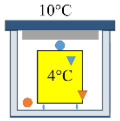	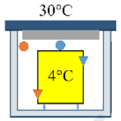	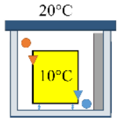	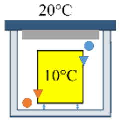	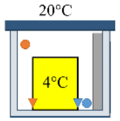	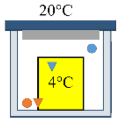	
Core temperature	Average	5.8 (5.6,6.0)	5.4 (5.3,5.4)	7.8	7.4	4.3	7.2	9.3	8.0	5.8 (5.7,5.8)	5.6 (5.4,5.7)	0.19
	Minimum	4.5 (4.2,4.8)	4.6 (4.5,4.6)	6.2	5.4	3.5	6.2	7.4	7.2	4.5 (4.4,4.6)	4.2 (4.1,4.3)	-
	Maximum	6.8 (6.6,7.1)	6.4 (6.3,6.4)	9.5	9.4	4.9	8.4	10.9	9.1	6.5 (6.4,6.6)	7.0 (6.8,7.1)	-
Surface temperature	Average	6.3 (6.1,6.5)	5.5 (5.3,5.7)	8.1	8.5	4.6	7.6	9.0	8.1	6.0 (6.1,5.9)	5.7 (5.6,5.8)	0.22
	Minimum	4.3 (4.1,4.5)	4.6 (4.4,4.7)	5.8	5.2	3.9	5.9	6.0	6.9	3.7 (3.4,3.9)	4.4 (4.2,4.5)	-
	Maximum	7.7 (7.3,8.1)	6.6 (6.4,6.9)	9.9	10.7	5.2	9.1	11.0	9.2	7.5 (7.2,7.8)	7.2 (7.0,7.3)	-
Internal air temperature	Average	6.6 (6.2,7.0)	5.7 (5.7,5.7)	8.5	10.0	4.7	9.1	8.7	8.0	6.4 (6.0,6.7)	5.6 (5.5,5.7)	0.38
	Minimum	2.6 (1.5,3.6)	4.5 (4.4,4.6)	4.7	4.6	3.5	5.2	4.1	6.3	1.6 (1.2,2.0)	4.4 (4.4,4.4)	-
	Maximum	8.6 (7.7,9.6)	7.0 (6.9,7.2)	12.2	13.3	5.2	10.0	10.7	9.1	8.9 (8.9,8.9)	7.0 (6.9,7.0)	-
	**SD	2.2	1.1	3.0	3.0	0.5	1.6	2.3	0.9	2.5	1.0	-

* ▼and▼ represent the coldest and warmest locations in the test product, respectively while ● and ● signify the coldest and warmest locations in the air, respectively.

** SD = Standard Deviation (°C). For a given condition (each column), SD represents the variation of air temperature among 13 measurement positions. For a given temperature (same row), SD represents the variation of temperature measured at 4 positions between 2 replications.

*** The values in parenthesis were the results of each replication.

Declaration of interests

☒ The authors declare that they have no known competing financial interests or personal relationships that could have appeared to influence the work reported in this paper.

☐ The authors declare the following financial interests/personal relationships which may be considered as potential competing interests: